

## A case study of cascade supercritical CO<sub>2</sub> power cycle for waste heat recovery from a small gas turbine

Davide Bonalumi, Antonio Giuffrida<sup>\*</sup>, Federico Sicali

Politecnico di Milano – Dipartimento di Energia, Via R. Lambruschini 4, 20156 Milano, Italy

### ARTICLE INFO

#### Keywords:

Gas turbine  
Single heated cascade cycle  
supercritical CO<sub>2</sub>  
Waste heat recovery

### ABSTRACT

Among the technological solutions that can be applied to waste heat recovery, the supercritical CO<sub>2</sub> (sCO<sub>2</sub>) cycle represents an innovative option. This work studies the performance of the single heated cascade sCO<sub>2</sub> cycle as the bottomer power system of a 5 MW-class gas turbine and follows a former study of the authors about the partial heating cycle. A number of parametric analyses has been carried out with attention paid to the selection of (i) minimum and maximum CO<sub>2</sub> pressures, based on a compressor Mach number selected to avoid highly loaded turbomachinery, (ii) maximum CO<sub>2</sub> temperature, and (iii) specific design parameters such as temperature difference at the cold side of the primary heater, recuperator effectiveness and single-stage radial-type turbine efficiency, the latter calculated according to Aungier's correlations by taking actual size and running conditions into account. The results of this study suggest that around 1500 kW of net electric power can be recovered by the single heated cascade sCO<sub>2</sub> cycle. This figure is not so different from the power output previously calculated for the partial heating cycle as well as the specific cost of the technology, which is around 2000 \$/kW, lower than a possible competing technology for waste heat recovery applications as the organic Rankine cycle. Nevertheless, the architecture investigated in this study needs two turbines which can rotate on the same shaft, but driving the compressor at the same rotational speed of the two turbines is not possible, as emerges from preliminary considerations about the size of the turbomachinery impellers.

### Introduction

Gas turbines are widely used technological solutions for power generation thanks to their high power density, compact size and high durability. Open cycle gas turbines are more widespread than closed cycle units due to the higher turbine inlet temperatures that the former can reach, making them more thermodynamically and economically efficient as well as compact. The temperature of the combustion gases at the inlet of the turbine within open cycle power systems can easily reach and currently exceed 1500 °C. However, as the exhaust gas temperature of the turbine is still high, there is a great amount of waste heat [1].

Nowadays, the steam Rankine cycle is the commonly available solution for waste heat recovery from gas turbines in a combined cycle architecture. The steam Rankine cycle has high thermal efficiency and excellent capacity for recovering heat from the exhaust gas, but the size of the cycle components is large because of the thermodynamic properties of water.

Unlike the steam Rankine cycle, the organic Rankine cycle (ORC) technology employs an organic fluid instead of water to convert energy.

In general, ORC has a better performance than the steam cycle for low-temperature waste heat recovery [2], but at high temperatures the organic fluid decomposition usually occurs. On the other hand, the supercritical CO<sub>2</sub> (sCO<sub>2</sub>) cycle can outperform the existing Rankine cycles: compared with the steam, sCO<sub>2</sub> has a higher density, resulting in compact turbomachinery and heat exchangers; compared with the organic fluid, sCO<sub>2</sub> has good physical properties, namely non-toxic, non-corrosive, non-flammable. Moreover, sCO<sub>2</sub> preserves unchanged all its main physical properties at temperatures typical for applications of waste heat recovery from gas turbines, unlike organic fluids which are useless above 350–400 °C [3].

#### Supercritical CO<sub>2</sub> cycles for waste heat recovery

Initially proposed by Feher [4] and Angelino [5] around fifty years ago, the supercritical CO<sub>2</sub> power cycle has sparked an interest which is increased rapidly in the last years [6], driven by the unique features of this technology as reported above. In detail, it is important not only to recover waste heat effectively in a single system, but also to keep high cycle efficiency [7]. Researchers have proposed several sCO<sub>2</sub> power

<sup>\*</sup> Corresponding author.

E-mail address: [antonio.giuffrida@polimi.it](mailto:antonio.giuffrida@polimi.it) (A. Giuffrida).

**Nomenclature**

A	area, m <sup>2</sup>
AMC	Acceleration Margin to Condensation
BOP	balance of plant
D	diameter, m
h	specific enthalpy, J·kg <sup>-1</sup>
HT	high temperature
HTH	high temperature heater
HTR	high temperature recuperator
HTT	high temperature turbine
LMTD	log mean temperature difference, K
LT	low temperature
LTH	low temperature heater
LTR	low temperature recuperator
LTT	low temperature turbine
$\dot{m}$	mass flow rate, kg·s <sup>-1</sup>
Ns	specific speed
ORC	organic Rankine cycle
p	pressure, Pa
P	power, W
Q	volumetric flow rate, m <sup>3</sup> ·s <sup>-1</sup>
$\dot{Q}$	heat transfer rate, W
REC	recuperator
SC	specific cost, \$·W <sup>-1</sup>
s	specific entropy, J·kg <sup>-1</sup> ·K <sup>-1</sup>
sCO <sub>2</sub>	supercritical carbon dioxide

SR	speed ratio
T	temperature, K
TM	turbomachinery
TOT	gas turbine outlet temperature, °C
u	peripheral velocity, m·s <sup>-1</sup>
U	overall heat transfer coefficient, W·m <sup>-2</sup> ·K <sup>-1</sup>
UA	product of overall heat transfer coefficient and heat transfer area, W·K <sup>-1</sup>
y	mass fraction

**Greek letters**

$\Delta$	difference
$\varepsilon$	effectiveness
$\eta$	efficiency
$\mu$	head coefficient
$\rho$	density, kg·m <sup>-3</sup>
$\varphi$	flow coefficient
$\omega$	rotational speed, rad·s <sup>-1</sup>

**Subscripts**

C	compressor
el	electric
in	inlet station
is	isentropic
out	outlet station
pol	polytropic
T	turbine

cycle layouts for waste heat recovery, which are novel and different from the early sCO<sub>2</sub> cycles [8] and usually consist of many heaters and turbines. These cycles can be generally divided into categories, namely “partial heating cycle”, “dual recuperated cycle”, “single heated cascade cycle” as well as “dual heated cascade cycle” [8,9].

The partial heating cycle is shown in Fig. 1a, where two sCO<sub>2</sub> streams are separated at the outlet of the compression system: the first extracts the exhaust heat in a low-temperature heater (LTH) and the second recovers heat in a recuperator (REC), then the two streams meet before

entering a high-temperature heater (HTH). By using this configuration, the temperature match in the heat transfer at the recuperator can be improved and the gas temperature at the outlet of the low-temperature heater (LTH) can be reduced. This power cycle has been studied in a number of works [9–13].

Fig. 1b shows the layout of the dual recuperated cycle [9,13]. Once again, the sCO<sub>2</sub> flow rate at the compressor outlet is always splitted into two streams. One stream sequentially absorbs heat in a low-temperature recuperator (LTR) and in the primary heater before expanding through a

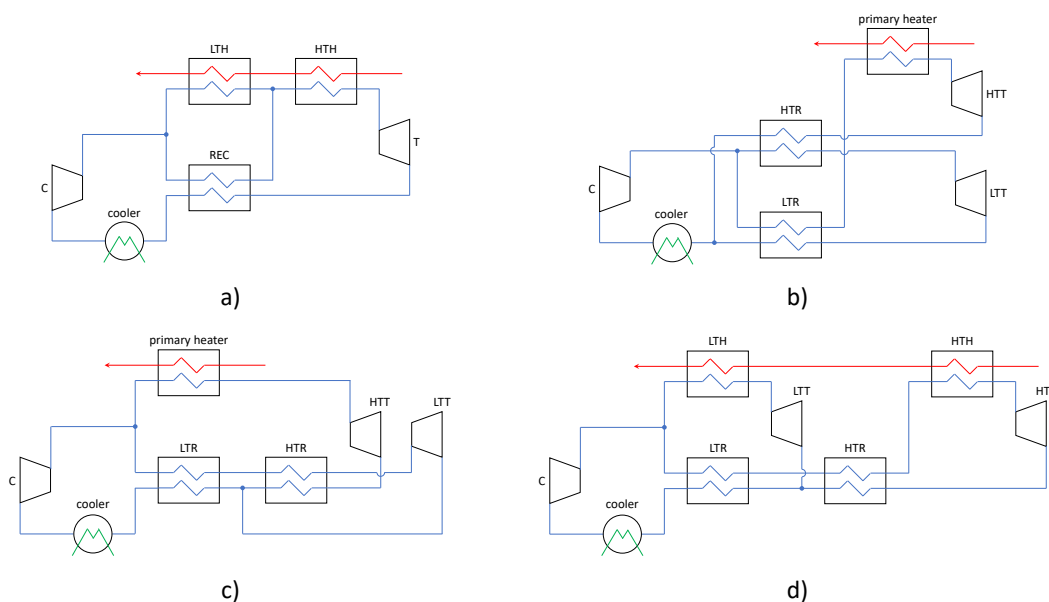


**Fig. 1.** Schematic layouts of sCO<sub>2</sub> cycles suitable for waste heat recovery: a) partial heating cycle, b) dual recuperated cycle, c) single heated cascade cycle, d) dual heated cascade cycle.

high-temperature turbine (HTT), whereas the second stream absorbs heat in the high-temperature recuperator (HTR) before expansion through a low-temperature turbine (LTT). Compared to the partial heating cycle, always three heat exchangers and one cooler are used in the dual recuperated cycle, but a second turbine is necessary.

Along with the layouts in Fig. 1a and 1b, other possible architectures for waste heat recovery applications can be considered as the ones originally proposed by Kimzey [14]. Fig. 1c shows the layout of the so-called single heated cascade cycle, with two recuperation processes before the cooler. Compared to the partial heating cycle in Fig. 1a, there is only one heater and one more turbine, but compared to the dual recuperated cycle in Fig. 1b it is possible to find the same number of components with a different arrangement. Actually, the two recuperators in the new cycle layout operate in series, whereas they are in parallel in Fig. 1b. This cycle has been widely investigated [9,13–16], though literature results are quite conflicting when comparing this cycle to other layouts. As a matter of fact, if Manente and Costa [13] calculated the superiority of the single heated cascade cycle in waste heat recovery compared to both the partial heating cycle and the dual recuperated cycle, Wright et al. [9] or Kim et al. [16] reported better performance for the partial heating cycle layout. In an effort to reduce the heat rejection in the cooler, Kimzey [14] also proposed the so-called dual heated cascade cycle, whose layout is shown in Fig. 1d. Once again, the two recuperators are arranged in series. This cycle architecture allows for a slightly higher flow rate through the cold side of the low-temperature recuperator (LTR), which causes a slightly larger amount of heat to be recuperated from the turbine outlet streams. The main difference from the single heated cascade cycle is that the hot exhaust gas is used to heat the high pressure sCO<sub>2</sub> on the way to both turbines. As the flow rate through the cold side of the low temperature recuperator is slightly higher, the temperature profile tracks a little bit more closely. Actually, the layout in Fig. 1d is more efficient than the one in Fig. 1c [15,16]. Other more complex cycle architectures may be found in literature [15–18], even including intercooled compression, but the improvements are quite marginal compared to the performance of the dual heated cascade cycle (see Fig. 1d).

Bottoming solutions to recover flue gas waste heat by sCO<sub>2</sub> cycles are still the focus of current research. In detail, as reported by Yang et al. [19], the methods are mainly divided into (i) studies of a variety of sCO<sub>2</sub> cycles, optimized to select the preferable layout by comparing the values of the objective functions, and (ii) improvements of the existing sCO<sub>2</sub> cycles by proposing a new cycle layout and determining the system performance based on the optimization of design variables.

#### Aim and novelty of the work

This work follows a previous paper dealing with the partial heating cycle (see Fig. 1a) as the bottomer of a 5 MW-class gas turbine [20]. Gas turbines with a few MW of power output are used for cogeneration, distributed power generation in both onshore and offshore industrial applications, industrial processes in the Oil & Gas industry, naval propulsion and mobile power generation. These power generation solutions are interesting for their compactness even if they are less efficient when compared to bigger turbomachinery, so a combined cycle architecture with a sCO<sub>2</sub>-based system would maintain the advantage of compactness and increase the overall efficiency.

In detail, the current work focuses on the single heated cascade cycle (Fig. 1c), as an interesting cycle architecture based on a simple layout with a limited number of components. According to the approach previously adopted by the authors [20], the selection of turbomachinery efficiency results from the suggestions by Aungier for radial-type compressors [21,22] and turbines [23] and a preliminary sizing of the impeller for compressor and turbines is also proposed. As a matter of fact, literature papers usually present performance cycle results based on turbomachinery efficiency values that could be inconsistent with the running specifications in terms of mass flow rate, enthalpy rise (for

compressors) or drop (for turbines), rotational speed, rotor dimensions, etc. Attention is also paid to the minimum pressure and temperature of the cycle, i.e. to the inlet conditions for the compressor, based on considerations related to the proximity to the critical CO<sub>2</sub> point. Economic considerations are also included as specific cost figures of the investigated technology.

#### Calculation assumptions for the sCO<sub>2</sub> cycle

The single heated cascade sCO<sub>2</sub> cycle is investigated as the bottomer of a small size gas turbine, whose main features are reported in Table 1 [24]. This gas turbine has the best simple cycle efficiency compared to competing machines of the same power output class and the exhaust gas temperature is suitable for steam generation in case of application for combined heat and power.

In the next paragraphs, some considerations are reported about (i) the sCO<sub>2</sub> conditions at the compressor inlet, (ii) the selection of the efficiency values for turbines and compressor, and (iii) a basis for the economic assessment of the sCO<sub>2</sub> cycle.

Use of the REFPROP database, as developed by the National Institute of Standards and Technology of the United States [25], has been made for the calculation of the thermodynamic properties of CO<sub>2</sub>, according to the equation of state proposed by Span and Wagner [26]. In detail, the REFPROP database has been integrated with the Microsoft Excel solver to calculate the sCO<sub>2</sub> cycle performance.

Some assumptions of heat exchanger effectiveness, temperature difference between the streams at the ends of the primary heater, fluid pressure drops, etc. are detailed in Table 2 for cycle calculations. Actually, the values assumed for recuperator effectiveness as well as for pressure drops in the sCO<sub>2</sub> paths through the heat exchangers are consistent with the suggestions by Weiland and Thimsen [27]. Auxiliary power demands are assumed based on previous works by the authors dealing with power cycles [28–30], whereas a slightly lower value has been selected for the organic-electrical efficiency for taking into account not only the electric generator but also the several auxiliaries such as gearbox systems, variable frequency drives, instrumentation and control systems, oil lubrication, oil cooling and purge gas management systems and CO<sub>2</sub> make-up systems.

On the other hand, specific considerations are necessary for setting further input assumptions as discussed in the next paragraphs.

#### Minimum cycle temperature and pressure

Calculations of sCO<sub>2</sub> cycles usually assume compressor inlet conditions relatively near to the two-phase region. In detail, the sCO<sub>2</sub> temperature is minimized for lower compression work and a minimum cycle temperature as low as 32 °C is selected in a number of literature works [31–38]. However, this near-critical inlet condition brings a few challenges for the compressor design and the potential for phase change through the compressor should be taken into account [39–41]. As a matter of fact, phase change could occur at the compressor inlet due to local flow acceleration and the related reduction in static pressure and temperature [42]. In the current work, reference to the Acceleration Margin to Condensation (AMC) is made. It is a non-dimensional criterion proposed by Monje et al. [39,40] to quantify the margin between the expected fluid properties in the inducer of the compressor and the saturation line.

**Table 1**  
Main features of the Kawasaki M5A gas turbine [24].

Electric output, kW	4710
Heat rate, kJ/kWh	11030
Thermal efficiency, %	32.6
Exhaust gas temperature, °C	511
Exhaust mass flow rate, kg/s	17.4

**Table 2**  
Assumptions for sCO<sub>2</sub> cycle calculations.

Recuperator effectiveness, %	90
ΔT on the heater cold side, K	20
Δp on the heater cold path, kPa	200
Δp on recuperator cold path, kPa	140
Δp on recuperator hot path, kPa	280
Consumption of cooling auxiliaries, kW <sub>el</sub> ·MW <sup>-1</sup>	15
Organic-electrical efficiency, %	90

Looking at Fig. 2a, where the total fluid conditions at the inlet of the compressor are set in the supercritical region, the isentropic static point where condensation would ideally occur is calculated by modelling an isentropic expansion down to the saturation pressure (or temperature) [39,40]. The Mach number resulting from this isentropic expansion is the Acceleration Margin to Condensation [39,40].

Fig. 2b shows AMC variations with compressor inlet pressure for three selected temperatures for the sake of simplicity. AMC values in Fig. 2b are calculated with reference to Fig. 2a as regards entropy values greater than the one at the critical point. In the case of lower entropy, the horizontal critical temperature is considered.

Although undesired phenomena of two-phase flows at the impeller throat should be avoided if the inlet Mach number is chosen far from the AMC, the proper AMC value should be selected based upon the particular specifications and operating strategy of the system under analysis. In particular, Monje et al. [39] suggested a threshold value of 0.6. Based on this figure, the minimum temperature for the sCO<sub>2</sub> cycle investigated in the current work is precautionarily set at 40 °C. As a matter of fact, this temperature results in a larger range of allowable pressures compared to lower temperatures. Thus, the compressor should not be exposed to the above-mentioned risks and cold carriers for sCO<sub>2</sub> cycle heat rejection are not required, without limiting the applicability only to some specific geographical areas.

In detail, after fixing the compressor inlet temperature at 40 °C, values in the range from the critical pressure (73.77 bar according to [26]) to 79.8 bar and from 89.3 to 95.6 bar could be selected for AMC values no less than 0.6.

#### Selection of turbomachinery efficiency

Three turbomachines are used in the power cycle schematically shown in Fig. 1c. Just single-stage turbomachines are considered in this work and the use of radial-inflow turbines is justified based on the relatively small size of the topping gas turbine. In particular, radial-inflow turbine efficiency and specific speed were related by Aungier [23]:

$$\eta_{is,T} = 0.87 - 1.07 \cdot (Ns_T - 0.55)^2 - 0.5 \cdot (Ns_T - 0.55)^3 \quad (1)$$

where the specific speed  $Ns$  for the turbine is given as

$$Ns_T = \omega_T \cdot \frac{\sqrt{Q_{out,s,T}}}{\Delta h_{is,T}^{0.75}} \quad (2)$$

According to Aungier' suggestion, turbine efficiency values from 0.85 to 0.87 can be achieved in the range of specific speeds between 0.41 and 0.68. In detail, a specific speed of 0.55 results in a turbine efficiency of 0.87, which is a more conservative assumption than 0.9 as adopted elsewhere [16] for a similar size system. Considering the turbine efficiency has a significant effect on cycle efficiency [43], two efficiency values are assumed in the next analysis, namely 0.87 and 0.85, even though two specific speeds are possible for the latter.

A blade tip speed ratio [23] is also introduced:

$$SR = \frac{u_T}{\sqrt{2 \cdot \Delta h_{is,T}}} = 0.737 \cdot Ns_T^{0.2} \quad (3)$$

representing the ratio between the peripheral impeller velocity and the spouting velocity, related to the enthalpy drop during isentropic expansion. The blade tip speed ratio based on Eq. (3) is shown in Fig. 3a along with the isentropic efficiency based on Eq. (1).

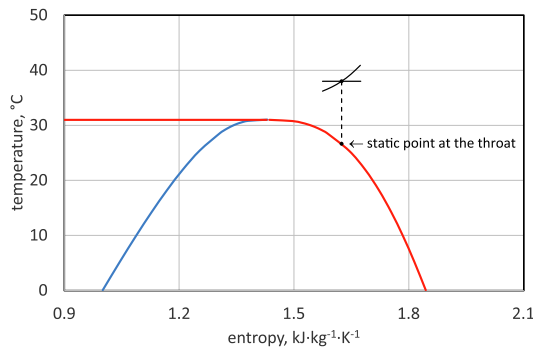
According to the equations above, the selection of the specific speed for the desired efficiency directly results in the blade tip speed ratio. After setting the maximum cycle temperature as well as inlet and outlet pressures for the high-temperature turbine, the spouting velocity at the denominator of Eq. (3) can be calculated, then the peripheral impeller velocity. As the sCO<sub>2</sub> flow rate through the high-temperature turbine results from an energy balance at the primary heater (see Fig. 1c), the HTT rotational speed can be obtained and, finally, the size of the turbine rotor. This approach is next repeated for the low-temperature turbine, after imposing both the turbines rotate on the same shaft.

Although both compressor and turbine can effectively rotate on the same shaft in the partial heating cycle (see Fig. 1a), as already adopted in a previous work [20], driving the compressor at the same rotational speed of the turbines may be challenging in a cascade cycle with more than one turbine. Specific considerations are duly reported in the next section 3.2.

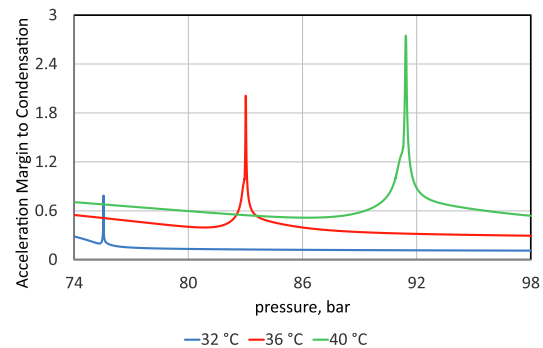
According to the preliminary design strategy for a centrifugal compressor stage proposed by Aungier [21,22], performance correlations in terms of the work input coefficient, i.e. the ratio between the head coefficient and the efficiency:

$$\frac{\eta_{pol,C}}{\eta_{pol,C}} = \frac{\Delta h_C}{u_C^2} = 0.68 - \left(\frac{\varphi_C}{0.37}\right)^3 + \frac{0.002}{\varphi_C} \quad (4)$$

and the polytropic head coefficient:



a)



b)

**Fig. 2.** Definition of the Acceleration Margin to Condensation, adapted from [34], on the left, along with values depending on the pressure at compressor inlet for three selected temperatures, on the right.

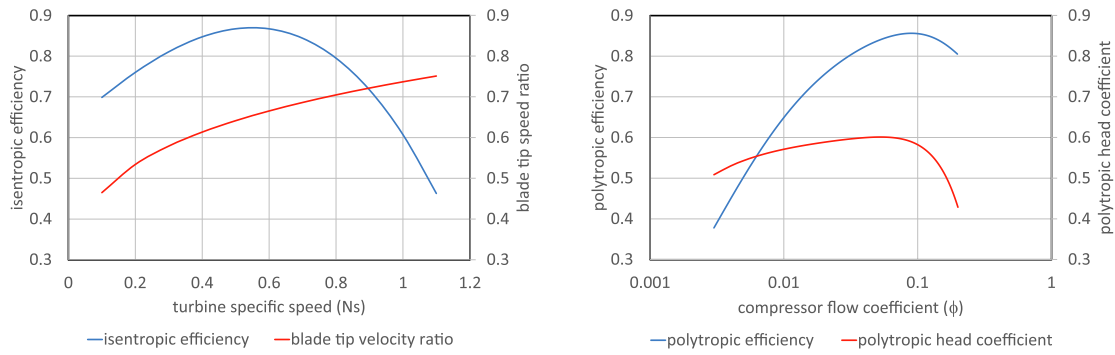


Fig. 3. Isentropic efficiency and blade tip speed ratio for the radial-inflow turbine (on the left) [23] and polytropic efficiency with the head coefficient for the centrifugal compressor (on the right) [21,22].

$$\mu_{pol,C} = 0.59 + 0.7 \cdot \varphi_C - 7.5 \cdot \varphi_C^2 - \frac{0.00025}{\varphi_C} \quad (5)$$

are functions of the flow coefficient  $\varphi_C$  defined as.

$$\varphi_C = \frac{4 \cdot \dot{Q}_{in,C}}{\pi \cdot D_C^2 \cdot \mu_C} \quad (6)$$

Both Eqs. (4) and (5) refer to a compressor architecture with open impeller and vaned diffuser.

Ultimately, based on Eq.(6) as well as on the mass flow rate and the rotational speed of the turbines from the above-mentioned calculations, a preliminary sizing of the compressor impeller diameter is possible.

#### Cost assessment of system components

The approach proposed by Wright et al. [9,44] is considered for an economic assessment of the sCO<sub>2</sub> power system. In detail, the cycle components are grouped into two categories: (i) turbomachinery plus auxiliary balance-of-plant (BOP) components and (ii) heat exchangers.

The first category includes turbines, compressors, seals and bearings, gearbox systems, generator, motors, variable frequency drives, piping, skids, instrumentation and control systems, oil lubrication, oil cooling and purge gas management systems and CO<sub>2</sub> make-up systems [9,44]. These costs for a first-of-a-kind system are estimated as proportional to the net power production.

As regards the heat exchangers, one primary heater, two recuperators and one cooler are included in the schematic layout of Fig. 1c. The specific cost for each typology of heat exchanger is reported in Table 3 and is assumed to be proportional to the UA parameter, where U is the overall heat transfer coefficient and A is the heat transfer area:

$$UA = \frac{\dot{Q}}{LMTD} \quad (7)$$

$\dot{Q}$  is the heat transfer rate and LMTD is the log mean temperature difference across the heat exchanger calculated by the thermal energy balance. Actually, the non-linear trends of the thermal profiles are taken into account to provide a proper value for UA. Thus, as adopted elsewhere [17], each heat exchanger is divided into a number of segments to calculate more precisely the temperature profiles and the overall LMTD is calculated based on  $\dot{Q}_j$  and LMTD<sub>j</sub> of the single segments:

Table 3

Cost assumptions for the components of the sCO<sub>2</sub> cycle [9,44].

Component	Specific cost	Cost unit
turbomachinery plus auxiliary BOP	1000	\$.kW <sup>-1</sup>
primary heater	5000	\$.kW <sup>-1</sup> .K
recuperator	2500	\$.kW <sup>-1</sup> .K
cooler	1700	\$.kW <sup>-1</sup> .K

$$LMTD = \left( \frac{1}{\dot{Q}} \cdot \sum_j \frac{\dot{Q}_j}{LMTD_j} \right)^{-1} \quad (8)$$

Ultimately, based on each component cost, a specific figure in \$.kW<sup>-1</sup> results for the selected sCO<sub>2</sub> cycle.

Although the cost uncertainty in Table 3 is estimated to be  $\pm 30\%$ , it is expected that the specific cost should even reduce as a production line is established [9,44].

#### Results and discussion

The performance of the investigated single heated cascade sCO<sub>2</sub> cycle is presented in this section as the result of a number of analyses focusing on the effects of (i) the minimum cycle pressure, (ii) the maximum cycle temperature, (iii) the temperature difference at the cold side of the primary heater as well as (iv) different effectiveness values for both the low- and the high-temperature recuperators.

Results are presented after imposing the highest isentropic efficiency for the high-temperature turbine (0.87 according to Aungier) since it receives higher enthalpy fluid with the possibility of producing more mechanical work. However, further considerations are included as regards a reduced expansion efficiency at the high-temperature turbine. As a matter of fact, it is not possible to set the same efficiency for both the high- and the low-temperature turbines throughout the calculations if they are assumed to rotate on the same shaft. According to Eq. (2), different mass flow rate distribution through the two expanders and different enthalpy drops cause different Ns values for the two turbines in spite of the same rotational speed. The expansion efficiency for the low-temperature turbine obviously results from Eq. (1), based on its specific speed.

The calculation procedure determines the maximum cycle pressure based on the fixed compressor Mach number and the splitting fraction at the compressor outlet (see Fig. 1c) results from the maximization of the net electric power. However, some difficulties come to light when running all the turbomachines at the same rotational speed. Actually, the rotational speed of the turbines is high and the resulting size of the impeller is sufficiently small. If this result is acceptable for the two turbines, it is difficult to drive the compressor at the same speed of the turbines for effectively accommodating and processing the total flow rate. As a matter of fact, based on a preliminary sizing of the compressor [45], there is serious risk of choking phenomena at the inlet of the impeller as well as of distorted velocity triangles. Thus, a lower speed is imposed for the compressor by introducing a reduction factor set equal to 2.

In detail, all the figures presented in the following sections result from the assumption of 0.85 for the compressor Mach number, calculated as the ratio between the impeller peripheral speed and the speed of sound of the working fluid at the compressor inlet. Indeed, a similar

value of the compressor Mach number (0.86) is reported in recent researches by Romei et al. [46,47], investigating a centrifugal compressor for sCO<sub>2</sub>-based applications operating in near-critical conditions. On the other hand, the single-stage compressor could be heavily loaded if the minimum sCO<sub>2</sub> cycle pressure is set too low. Actually, based on previous calculations [20], the range between the critical pressure and 79.8 bar for an AMC value of 0.6 resulted in an excessively high compressor Mach number compared to the value of around 1.25 reported by Modekurti et al. [48] as a limit value for a single-stage compression unit.

#### Effects of the minimum sCO<sub>2</sub> pressure

This section focuses on the effects of the minimum sCO<sub>2</sub> cycle pressure after setting the efficiency of the high-temperature turbine at 0.87 for the best cycle performance.

According to the assumption of a minimum sCO<sub>2</sub> cycle temperature of 40 °C, two ranges for the minimum cycle pressure could be considered throughout the thermodynamic analysis for an AMC value no less than 0.6 at the compressor inlet (see Fig. 2b). Limiting to the range from 89.3 to 95.6 bar, Fig. 4a and 4b show the net electric power and the sCO<sub>2</sub> cycle specific cost for two maximum cycle temperatures, namely 400 °C and 480 °C, the latter due to the TOT of the topper cycle equal to 511 °C (see Table 1). It is possible to appreciate that the minimum sCO<sub>2</sub> cycle pressure seriously affects the two results. As a matter of fact, the highest value in the investigated pressure range is decisively to be selected for both the highest power output and the lowest specific cost. Both these results are achieved with a clear trend despite the maximum cycle temperature.

Based on a specific aerodynamic load of the turbomachinery as the result of the fixed value for the compressor Mach number (0.85), Fig. 5 shows the higher the minimum cycle pressure the higher the pressure ratio of the compressor. This result is also justified by the speed of sound at the compressor inlet, which increases with the pressure selected in the investigated range. In detail, in case of setting 480 °C as the maximum cycle temperature, the pressure ratio rises from 2.06 to 2.77, the impeller diameter of the compressor reduces but the rotational speed increases. These trends remain similar even in the case of considering lower maximum temperatures.

According to these preliminary results, the minimum cycle pressure is always fixed at 95.6 bar in the next sections.

#### Effects of the maximum sCO<sub>2</sub> temperature

The second analysis is carried out by focusing on the maximum cycle temperature, which is varied from 400 °C up to 480 °C. The minimum cycle pressure is set at 95.6 bar according to the main results in section 3.1. Fig. 6a shows that the net electric power increases with the

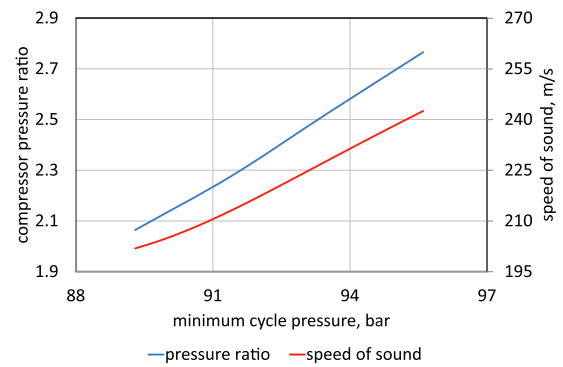


Fig. 5. Compressor pressure ratio (maximum cycle temperature equal to 480 °C) and speed of sound at compressor inlet as functions of the minimum cycle pressure.

maximum cycle temperature, even though a different trend is accomplished for the specific cost, which presents a clear minimum as reported in Fig. 6b. The results in both Fig. 6a and 6b are proposed for two values of the isentropic efficiency of the HT turbine, 0.85 and 0.87 respectively. When considering lower HTT efficiency, a 3.8 percentage point reduction in net electric power is evident in case of maximum cycle temperature of 480 °C. However, the reduction is heavier when setting lower maximum cycle temperatures. Moreover, the negative effects of lower HTT efficiency can also be appreciated by looking at Fig. 6b.

The thermal power extracted from the exhaust gas is almost the same because the exhaust gas flow rate and its temperature are fixed (see Table 1) and the temperature at the stack does not experience significant variations. In detail, an effectiveness of 95.6% is always calculated for the primary heater as the results of the fixed temperature difference at the cold side (20 K). As shown in Fig. 7a, the sCO<sub>2</sub> mass flow rate delivered by the compressor, which is calculated by applying the energy balance on the primary heater, reduces when the maximum cycle temperature varies from 400 °C to 480 °C. A similar trend is achieved for the sCO<sub>2</sub> stream passing through the primary heater, despite the value of the isentropic efficiency of the HT turbine.

Limiting to the result set achieved with the highest isentropic efficiency of the HT turbine (0.87), the higher the maximum cycle temperature, the lower the heat rejection by the cooler, mainly due to the reduction of the sCO<sub>2</sub> mass flow rate, so the mechanical power clearly increases as the result of the input thermal power minus the rejected thermal power. As regards the two recuperators, the internal thermal recovery is as higher as the maximum cycle temperature increases. The heat transfer rate increases with the maximum cycle temperature in both recuperators: it is very slight for the HT recuperator, but more evident

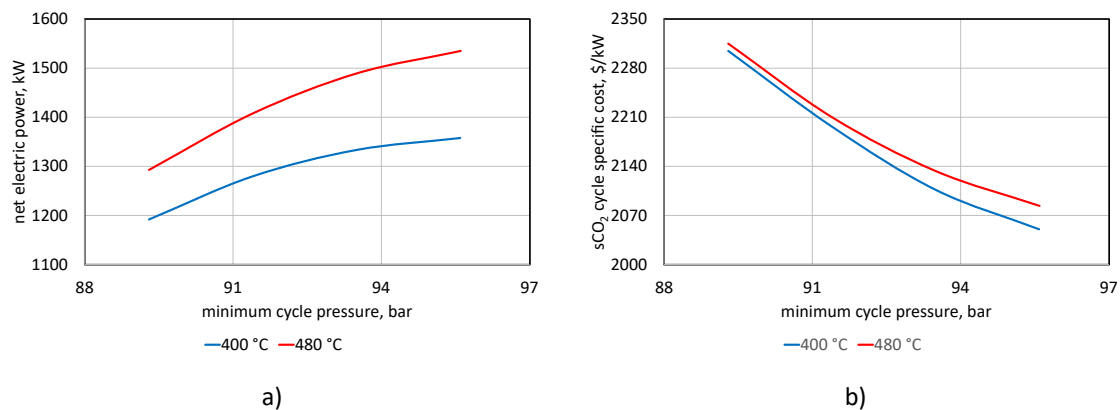


Fig. 4. Net electric power output (on the left) and specific cost (on the right) as functions of the minimum cycle pressure for two values of maximum cycle temperature.

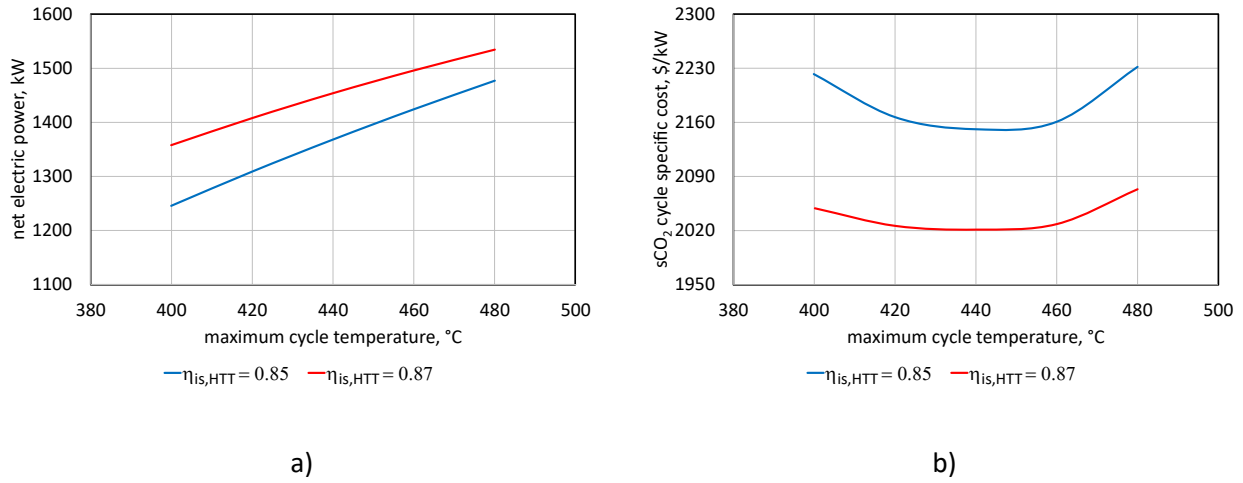


Fig. 6. Net electric power output (on the left) and specific cost (on the right) as functions of the maximum cycle temperature for two efficiency values of the HT turbine.

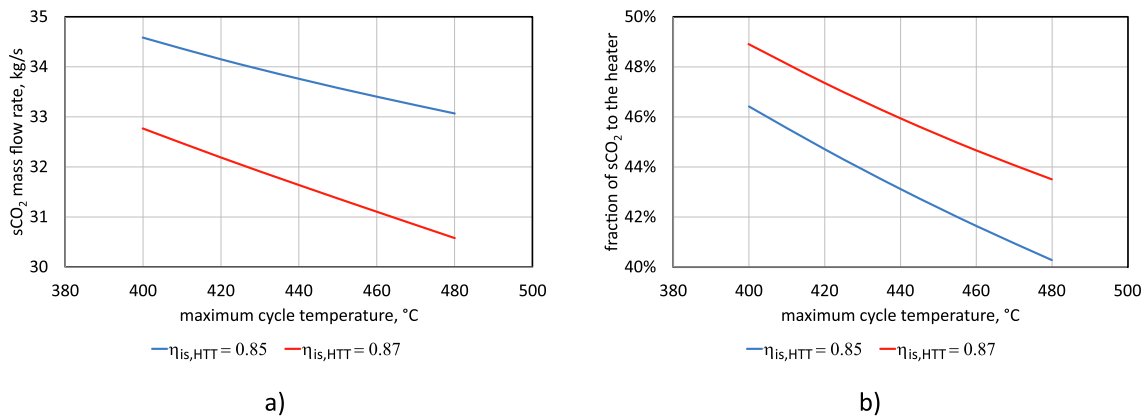


Fig. 7. sCO<sub>2</sub> mass flow rate delivered by the compressor (on the left) and fraction of sCO<sub>2</sub> passing through the heater (on the right) as functions of the maximum cycle temperature for two efficiency values of the HT turbine.

for the LT recuperator, as shown in Fig. 8a. Actually, the higher the maximum cycle temperature, the higher the sCO<sub>2</sub> temperature at the outlet of the LT turbine, resulting in hotter fluid at the inlet of the low-pressure side of the LT recuperator after the mixing process (see Fig. 1c). As a consequence, the heat transfer rate for this component rises. On the

other hand, the increment of the heat transfer rate for the HT recuperator is less evident because of the contrast between the higher sCO<sub>2</sub> temperature at the outlet of the HT turbine and the higher sCO<sub>2</sub> temperature from the LT recuperator.

A break-down of the heat exchanger cost is also reported in Fig. 8b,

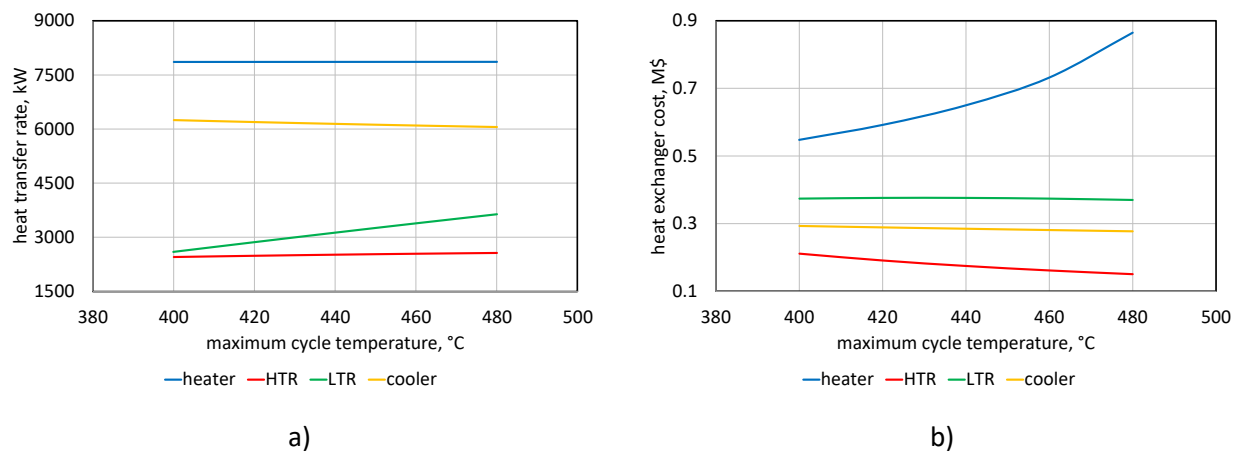


Fig. 8. Heat transfer rate (on the left) and cost (on the right) of the heat transfer equipment in the sCO<sub>2</sub> cycle as functions of the maximum cycle temperature (isentropic efficiency of the HT turbine equal to 0.87).

according to the approach based on the calculated UA value as presented in section 2.3. The most expensive component is always the primary heater. As the maximum cycle temperature increases, the thermal power recovery does not change, the temperature difference at the hot side of the heater decreases as well as the logarithmic mean temperature difference, so the increasing UA value drives the heater cost up.

Looking at the results in Fig. 9, the trend of the specific cost in Fig. 6b can be explained. As a matter of fact, it is sufficient to compare the slopes of the power and cost curves, the first with a modest downward concavity and the second with a more evident upward concavity for higher maximum cycle temperatures. Thus, the presence of a minimum specific cost in the investigated range of maximum cycle temperatures is justified.

Figs. 8 and 9 limit the analysis to the case of the HT turbine with the maximum isentropic efficiency, but similar trends result when reducing this efficiency from 0.87 to 0.85.

Attention is now paid to the turbomachinery. Starting from the case where the HT turbine has an isentropic efficiency of 0.87, the corresponding specific speed is 0.55 according to Eq. (1). The relation between the rotational speed and the specific speed is the following:

$$\omega_{HTT} = N_{SHTT} \cdot \frac{\Delta h_{is,HTT}^{0.75}}{\sqrt{Q_{out,HTT}}} = N_{SHTT} \cdot \frac{\Delta h_{is,HTT}^{0.75}}{\sqrt{\frac{(1-y) \cdot m}{\rho_{out,HTT}}}} \quad (9)$$

where y is the fraction of sCO<sub>2</sub> at the outlet of the compressor flowing through the low-temperature recuperator.

The higher the temperature at the turbine inlet, the higher the isentropic enthalpy drop. In addition, considering the lower flow rate through both the heater and the HT turbine, due to higher maximum cycle temperature, the rotational speed increases considerably.

The specific speed of the LT turbine:

$$N_{SLT} = \omega_{LTT} \cdot \frac{\sqrt{\frac{y \cdot m}{\rho_{out,LTT}}}}{\Delta h_{is,LTT}^{0.75}} \quad (10)$$

increases from 0.61 to 0.68, due to the higher rotational speed ( $\omega_{LTT} = \omega_{HTT}$ ) and the slightly larger flow rate through the LT turbine than through the HT turbine, even though the isentropic enthalpy drop increases. Thus, the isentropic efficiency of LT turbine reduces from 0.866, in case of maximum cycle temperature of 400 °C, down to 0.851 for higher cycle temperatures according to the trend proposed by Aungier (see Fig. 3a).

The peripheral velocity of the HT turbine rotor ranges between 305 and 328 m/s and increases with higher maximum cycle temperatures. Actually, the speed ratio in Eq. (3) depends on the specific speed, which is fixed ( $N_{SHTT} = 0.55$ ) to achieve the desired efficiency ( $\eta_{is,HTT} = 0.87$ ): the higher the maximum cycle temperature, the higher the enthalpy drop, i.e. the spouting velocity, the higher the peripheral speed. Despite the speed ratio increases for the LT turbine, lower velocity values are

calculated (262–288 m/s) due to the lower available enthalpy drop.

The Mach numbers for the two turbines do not significantly vary, since the variations of speed of sound at the inlet of the machine contrast the higher peripheral velocity.

Focusing on the compressor, the isentropic enthalpy head does not experience significant variations as well as the isentropic efficiency, ranging between 0.801 and 0.816, while the specific speed increases from 0.48 to 0.53 as the maximum cycle temperature rises. The peripheral velocity of the compressor impeller keeps constant because of the fixed machine Mach number and inlet conditions, then the impeller diameter reduces for higher maximum cycle temperatures and the same trend can be appreciated as regards both turbines. Finally, also the flow coefficient ( $\varphi_C$ ) rises with the maximum cycle temperature, from 0.034 to 0.04 according to Aungier's approach, despite a small reduction of the inlet volumetric flow rate because of the second power of the impeller diameter included in Eq. (6).

Fig. 10a and 10b show specific results for the turbomachinery, in case of isentropic efficiency of the HT turbine equal to 0.87. In particular, the rotational speed may be as high as around 90 krpm, which is not unusual for sCO<sub>2</sub> turbines. As a matter of fact, if Lv et al. [49] designed a rotational speed of 80 krpm, there are literature works proposing the aerodynamic design of radial-inflow turbines even rotating up to 160 krpm [50,51].

Nevertheless, some results are presented in the previous figures even in the case of lower isentropic efficiency of the HT turbine (0.85 instead of 0.87), so attention is paid to the turbomachinery results in the following.

Based on the Aungier's approach, two values of specific speed can be selected for an isentropic efficiency of 0.85, namely 0.41 and 0.68. The lowest specific speed is considered here because it (i) results in higher efficiency values for the LT turbine and (ii) leads to lower rotational speeds. As a matter of fact, when setting  $N_{SHTT} = 0.41$ , the specific speed of the LT turbine ranges from 0.48 to 0.55 with efficiency greater than 0.85 (see Fig. 3a), whereas if  $N_{SHTT} = 0.68$ , the specific speed of the LT turbine would range from 0.70 to 0.76 with efficiency less than 0.85 (see Fig. 3a). On the other hand,  $N_{SHTT} = 0.68$  would result in lower dimensions, insufficient to accommodate the flow rate neither through the two turbines nor through the compressor. Fig. 11a shows lower rotational speeds compared to Fig. 10a, an isentropic efficiency of the LT turbine always greater than 0.85, but poor performance for the compressor, whose flow coefficient ( $\varphi_C$ ) ranges now from 0.019 to 0.024 (see Fig. 3b). As a result of lower rotational speeds, impeller diameters in Fig. 11b are larger compared to the case reported in Fig. 10b.

Although the results in Fig. 6a achieved in case of lower HTT isentropic efficiency may be trivial, rotational speeds and turbomachinery impeller diameters shown in Figs. 10 and 11 highlight the importance of including an even basic turbomachinery behavior in the assessment of the sCO<sub>2</sub> cycle performance. Of course, specific optimizations are always possible though outside the scope of the current work.

### Effects of the flue gas temperature

Attention is now paid to the final flue gas temperature or to the temperature difference at the cold side of the primary heater, which is varied in the range 10–30 K. As regards the main calculation assumptions, the maximum cycle temperature is set at 480 °C, based on the former analysis, whereas the other inputs are not varied. Again, the calculation is oriented to find the splitting fraction at the compressor outlet for the maximization of the net electric power.

When the temperature difference at the cold side of the primary heater varies, no sensible effects can be appreciated for the turbomachinery in terms of efficiency, aerodynamic load, i.e. Mach number, as well as rotational speeds and impeller diameters. On the other hand, the lower the temperature difference at the cold side of the primary heater the higher the amount of thermal power recovery from the heat source and the higher the net electric power production, with an almost linear

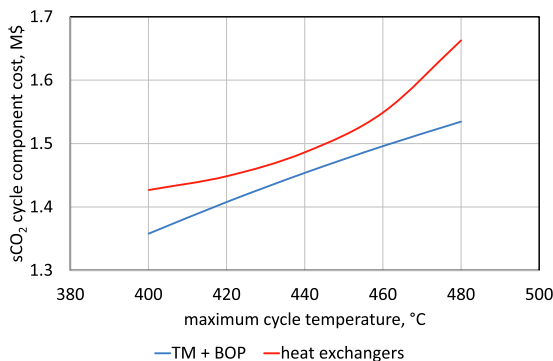


Fig. 9. Costs of the sCO<sub>2</sub> cycle components as a function of the maximum cycle temperature (isentropic efficiency of the HT turbine equal to 0.87).

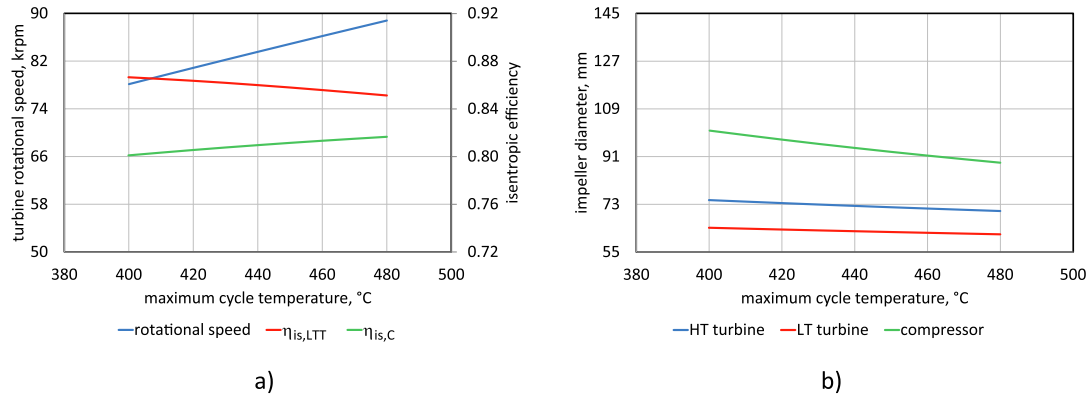


Fig. 10. Turbine rotational speed with isentropic efficiency of LT turbine and compressor (on the left) and turbomachinery impeller diameters (on the right) as functions of the maximum cycle temperature (isentropic efficiency of the HT turbine equal to 0.87).

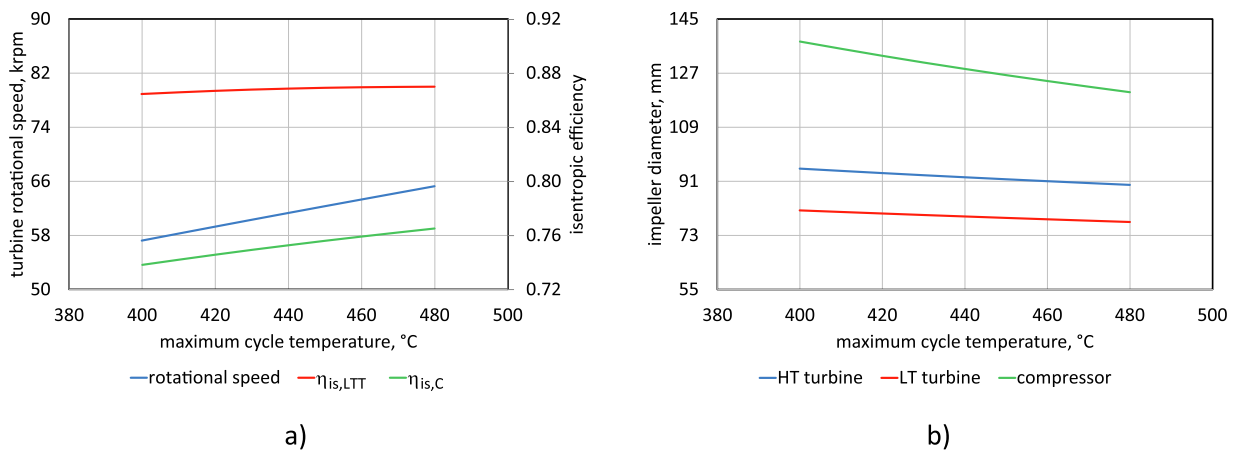


Fig. 11. Turbine rotational speed with isentropic efficiency of LT turbine and compressor (on the left) and turbomachinery impeller diameters (on the right) as functions of the maximum cycle temperature (isentropic efficiency of the HT turbine equal to 0.85 for  $N_{s_{HTT}} = 0.41$ ).

trend as shown in Fig. 12a. Actually, the  $sCO_2$  flow rate slightly increases because of lower flue gas temperatures.

Fig. 12b shows the  $sCO_2$  cycle specific cost which increases for lower temperature differences at the cold side of the primary heater. This trend can be justified by paying attention to the primary heater. As reported in Fig. 13, when less warm gas is exhausted, the reduction of the

temperature differences along the primary heater and the increasing thermal power recovery result in a sharp increase of the UA value as well as of the related component cost.

The primary heater effectiveness increases as the temperature difference at the cold side decreases and the slope of the curve in Fig. 13 is more significant in case of  $\Delta T$  values less than 25 K. When  $\Delta T$  is set at the

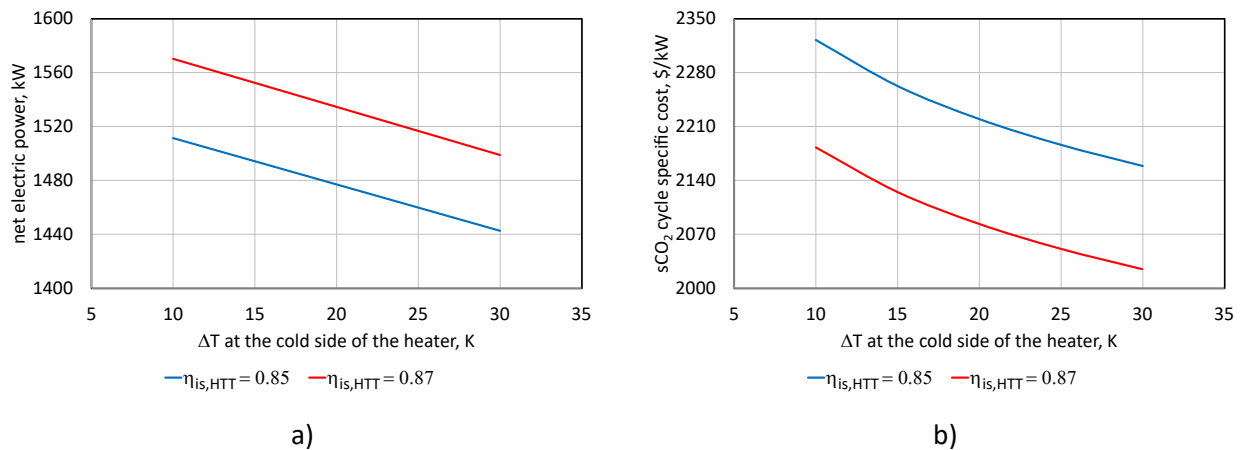
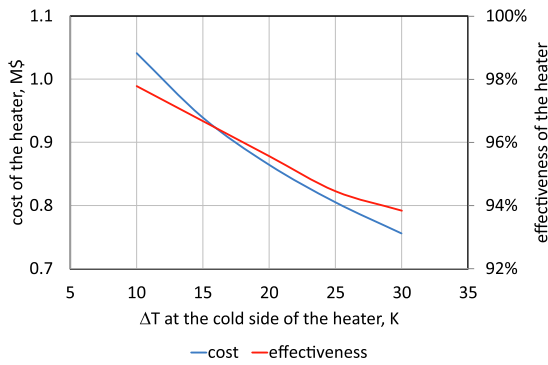


Fig. 12. Net electric power output (on the left) and specific cost (on the right) as functions of the temperature difference at the cold side of the primary heater for two efficiency values of the HT turbine.



**Fig. 13.** Cost and effectiveness of the primary heater depending on the temperature difference at the cold side of the heat exchanger (isentropic efficiency of the HT turbine equal to 0.87).

lowest value (10 K) the effectiveness approaches 98%, which is a challenging performance that heat exchangers for sCO<sub>2</sub> applications should be able to achieve [52,53]. On the other hand, the cooler has about the same cost in the investigated range of ΔT and no sensible variation is calculated for the costs of the two recuperators. The turbomachinery and BOP cost always follows the same trend of the net electric power.

Differently from the previous analysis focusing on the maximum cycle temperature, the specific cost for the current case is monotonic and its trend is in line with the one shown in Fig. 13 for the primary heater. As a matter of fact, the variation of the total equipment cost is more significant if compared to the net electric power.

*Effects of the recuperator effectiveness*

The previous sections have reported results achieved after imposing fixed values (90% as reported in Table 2) for the effectiveness of the two recuperators. Thus, the results of further investigations are reported in this section by setting different effectiveness values and imposing the maximum cycle temperature equal to 480 °C and the temperature difference at the cold side of the primary heater equal to 20 K.

Fig. 14a and 14b show the results of the electric power output and of the specific cost, respectively.

Based on the results in Fig. 14a, the same net electric power could be obtained with the combination of different effectiveness values, with a constant focus on the specific cost. Higher effectiveness values result in higher electric power production, with an almost linear trend as shown in Fig. 14a. The ε parameter has a more remarkable effect if related to the LT recuperator. Actually, as anticipated in Fig. 8a, the heat transfer rate of the LT recuperator is greater compared to the HT recuperator, as

well as its cost (see Fig. 8b). Looking at the trends in Fig. 14b, the specific cost rises more than proportionally when increasing the effectiveness of the LT recuperator. Similar results are achieved for higher effectiveness of the HT recuperator, even though differences are marginal. As a matter of fact, more significant variations in the specific cost can be appreciated when ε<sub>HTR</sub> moves from 92.5% to 95%. These trends agree with others reported in literature [27,54].

Specific turbomachinery results are not reported for the sake of brevity as they are not significantly influenced by the effectiveness variations of the two recuperators.

*Comparisons with the partial heating cycle*

According to a greater set of parameters that can be varied compared to the partial heating cycle [20], the single heated cascade cycle seems to be more beneficial for waste heat recovery applications. After setting similar calculation hypotheses (compressor Mach number at 0.85, recuperator effectiveness at 0.9, temperature difference at the cold side of the primary heater at 20 K, etc.) as the ones adopted in a former paper [20], Fig. 6a indicates 1535 kW for the maximum power output and Fig. 6b shows a specific cost of 2083 \$/kW. These results are almost similar to 1572 kW and 2165 \$/kW of the case study focusing on the partial heating cycle [20], as limited variations can be appreciated. Nevertheless, a few considerations are necessary for a fairer comparison.

- Maximum cycle temperatures between 400 °C and 480 °C are considered in the current analysis (section 3.2), but a maximum temperature of around 340 °C has been calculated for the partial heating cycle as the result of electric power maximization [20].
- From a cycle layout point of view, two smaller turbines are present in the single heated cascade cycle and their rotational speed (78–88 krpm as shown in Fig. 10a) is higher than the one of the single turbine (around 53 krpm) as calculated for the partial heating cycle [20].
- No direct matching is possible for compressor and turbine shafts, since it has been anticipated that the compressor must rotate slowly compared to the two turbines. Thus, a gearing system [55] is necessary (i) to allow the turbines to rotate at the optimum rotational speeds, (ii) to drive the compressor accordingly, (iii) without neglecting the frequency of the electric generator, actually lower than the values reported in Fig. 10a or 11a.

On the other hand, in spite of specific technological issues, a comparison with another technology for waste heat recovery, i.e. the organic Rankine cycle, is proposed in terms of costs. In particular, the specific cost for the ORC technology is calculated as.

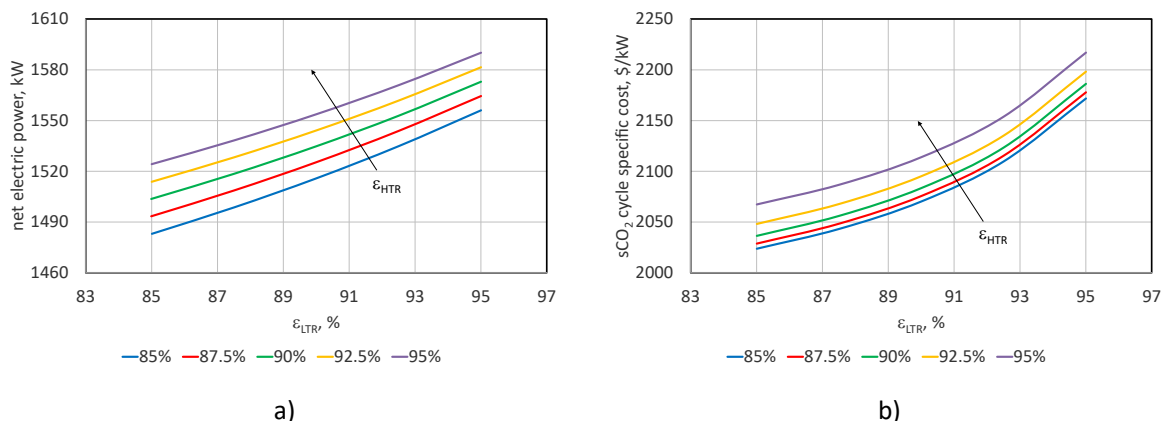


**Fig. 14.** Net electric power output (on the left) and specific cost (on the right) as functions of the effectiveness of both HT and LT recuperators.

$$SC_{ORC} = 19358 \cdot P_{el}^{-0.2703} \quad (11)$$

according to Baldasso et al. [56] who retrieved the cost estimations reported by Lemmens [57]. The specific cost in Eq. (11) is calculated as  $\$/kW^{-1}$  and  $P_{el}$  is the net electric power production in kW. According to the last formula, the specific cost of the sCO<sub>2</sub>-based technology investigated in this work can result around 22% lower compared to ORC figures, so the developments in this emerging field are really crucial for future technology readiness [58].

## Conclusions

A technical assessment of the single heated cascade sCO<sub>2</sub> cycle as the bottomer of a 5 MW-class gas turbine has been presented and supported with some cost indications.

Based on focused parametric analyses, attention has been paid to the proper selection of (i) minimum and maximum cycle pressures, after setting the compressor Mach number to avoid highly loaded turbomachinery, (ii) maximum cycle temperature, and (iii) design parameters including the temperature difference at the cold side of the primary heater, the effectiveness values of the two cycle recuperators and the efficiency of the high-temperature radial-inflow turbine, as the other turbomachinery efficiency values result from specific running conditions.

Around 1500 kW of net electric power can be recovered by the investigated bottoming cycle, with a specific cost of the technology of around 2000  $\$/kW$ . In detail, the last figure is lower compared to the specific cost of the organic Rankine cycle [56,57], as a possible competing solution for waste heat recovery applications, and highlights the potential of the sCO<sub>2</sub> power cycle technology.

The performance results presented and discussed in this work are not so different from the ones previously calculated for the partial heating cycle [20]. Actually, the single heated cascade cycle was found to produce slightly higher power output than the partial heating cycle, even though in case of heat recovery from waste gas at 600 °C [13]. Nevertheless, the cycle architecture here investigated does not allow to drive the compressor at the same rotational speed of the two turbines so the single heated cascade layout may result less interesting than the partial heating cycle architecture.

## CRedit authorship contribution statement

**Davide Bonalumi:** Conceptualization, Writing – original draft, Writing – review & editing. **Antonio Giuffrida:** Conceptualization, Methodology, Validation, Data curation, Writing – original draft, Writing – review & editing, Visualization, Supervision. **Federico Sicali:** Methodology, Software, Validation, Investigation, Data curation, Visualization.

## Declaration of Competing Interest

The authors declare that they have no known competing financial interests or personal relationships that could have appeared to influence the work reported in this paper.

## References

- [1] Gas Turbine World 2020 GTW Handbook, Pequot Publishing, vol. 35, 2020.
- [2] Loni R, Najafi G, Bellos E, Rajaeef F, Said Z, Mazlan M. A review of industrial waste heat recovery system for power generation with organic Rankine cycle: recent challenges and future outlook. *J Cleaner Prod* 2020;287:125070. <https://doi.org/10.1016/j.jclepro.2020.125070>.
- [3] Invernizzi CM, Bonalumi D. Thermal stability of organic fluids for Organic Rankine Cycle systems. In: "Macchi E, Astolfi M. , editor. Organic Rankine Cycle (ORC) Power Systems: Technologies and Applications. Woodhead Publishing; 2017". p. 121–51. <https://doi.org/10.1016/B978-0-08-100510-1.00005-3>.
- [4] Feher EG. The Supercritical Thermodynamic Power Cycle. *Energy Conversion* 1968;8(2):85–90. [https://doi.org/10.1016/0013-7480\(68\)90105-8](https://doi.org/10.1016/0013-7480(68)90105-8).
- [5] Angelino G. Carbon dioxide condensation cycles for power production. *J Eng Gas Turbines Power* 1968;90(3):287–95. <https://doi.org/10.1115/1.3609190>.
- [6] Yu A, Su W, Lin X, Zhou N. Recent trends of supercritical CO<sub>2</sub> Brayton cycle: Bibliometric analysis and research review. *Nucl Eng Technol* 2021;53(3):699–714. <https://doi.org/10.1016/j.net.2020.08.005>.
- [7] Liu L, Yang Q, Cui G. Supercritical carbon dioxide (s-CO<sub>2</sub>) power cycle for waste heat recovery: A review from thermodynamic perspective. *Processes* 2020;8(11):1461. <https://doi.org/10.3390/pr8111461>.
- [8] Crespi F, Gavagnin G, Sanchez D, Martinez GS. Supercritical carbon dioxide cycles for power generation: A review. *Appl Energy* 2017;195:152–83. <https://doi.org/10.1016/j.apenergy.2017.02.048>.
- [9] Wright SA, Davidson CS, Scammell WO. Thermo-economic analysis of four sCO<sub>2</sub> waste heat recovery power systems. *The 5th International sCO<sub>2</sub> Power Cycles Symposium*. 2016.
- [10] Kim YM, Sohn JL, Yoon ES. Supercritical CO<sub>2</sub> Rankine cycles for waste heat recovery from gas turbine. *Energy* 2017;118:893–905. <https://doi.org/10.1016/j.energy.2016.10.106>.
- [11] Ayub A, Sheikh NA, Tariq R, Khan MM, Invernizzi CM. Exergetic optimization and comparison of combined gas turbine supercritical CO<sub>2</sub> power cycles. *J Renewable Sustainable Energy* 2018;10(4):044703.
- [12] Sanchez Villafana ED, Bueno VM, Jr.. Thermo-economic and environmental analysis and optimization of the supercritical CO<sub>2</sub> cycle integration in a simple cycle power plant. *Appl Therm Eng* 2019;152:1–12.
- [13] Manente G, Costa M. On the conceptual design of novel supercritical CO<sub>2</sub> power cycles for waste heat recovery. *Energies* 2020;13(2):370. <https://doi.org/10.3390/en13020370>.
- [14] Kimzey G. Development of a Brayton bottoming cycle using supercritical carbon dioxide as the working fluid. *Electric Power Research Institute Report*; 2012, Palo Alto, CA:1–31.
- [15] Cho SK, Kim M, Baik S, Ahn Y, Lee JI. Investigation of the bottoming cycle for high efficiency combined cycle gas turbine system with supercritical carbon dioxide power cycle. *Proceedings of the ASME Turbo Expo* 2015. <https://doi.org/10.1115/GT2015-43077>.
- [16] Kim MS, Ahn Y, Kim B, Lee JI. Study on the supercritical CO<sub>2</sub> power cycles for landfill gas firing gas turbine bottoming cycle. *Energy* 2016;111:893–909. <https://doi.org/10.1016/j.energy.2016.06.014>.
- [17] Manente G, Fortuna FM. Supercritical CO<sub>2</sub> power cycles for waste heat recovery: a systematic comparison between traditional and novel layouts with dual expansion. *Energy Convers Manage* 2019;197:111777. <https://doi.org/10.1016/j.enconman.2019.111777>.
- [18] Lin X, Chen C, Yin L, Su W, Zhou N. Development of a novel dual heated cascade supercritical carbon dioxide cycle and performance comparison with existing two configurations for waste heat recovery. *Int J Energy Res* 2021;45(10):15389–408. <https://doi.org/10.1002/er.6811>.
- [19] Yang C, Deng Y, Zhang N, Zhang X, He G, Bao J. Optimal structure design of supercritical CO<sub>2</sub> power cycle for gas turbine waste heat recovery: A superstructure method. *Appl Therm Eng* 2021;198:117515. <https://doi.org/10.1016/j.applthermaleng.2021.117515>.
- [20] Bonalumi D, Giuffrida A, Sicali F. Thermo-economic analysis of a supercritical CO<sub>2</sub>-based waste heat recovery system. *Proceedings of the Italian National Congress ATI* 2021;312:08022.
- [21] Aungier RH. Centrifugal compressor stage preliminary design and component sizing. *Proceedings of the International Gas Turbine and Aero Engine Congress and Exposition* 1995. <https://doi.org/10.1115/95-GT-078>.
- [22] Centrifugal ARH. *Compressors - A Strategy for Aerodynamic Design and Analysis*. ASME Press; 2000.
- [23] Aungier RH. *Turbine aerodynamics - Axial-flow and radial-inflow turbine design and analysis*. ASME Press 2005.
- [24] Ishihara S, Terauchi K, Ikeguchi T, Ryu M. Development of high efficiency 5 MW class gas turbine - The Kawasaki M5A. *Proceedings of the ASME Turbo Expo* 2019. <https://doi.org/10.1115/GT2019-90773>.
- [25] <https://www.nist.gov/srd/refprop>, last access on December 13, 2021.
- [26] Span R, Wagner W. A new equation of state for carbon dioxide covering the fluid region from the triple-point temperature to 1100 K at pressures up to 800 MPa. *J Phys Chem Ref Data* 1996;25(6):1509–96. <https://doi.org/10.1063/1.555991>.
- [27] Weiland N, Thimsen D. A Practical Look at Assumptions and Constraints for Steady State Modeling of sCO<sub>2</sub> Brayton Power Cycles, *The 5th International sCO<sub>2</sub> Power Cycles Symposium*, 2016, <http://sco2symposium.com/papers2016/SystemModeling/102paper.pdf>.
- [28] Bonalumi D, Giuffrida A, Lozza G. A study of CO<sub>2</sub> capture in advanced IGCC systems by ammonia scrubbing. *Energy Procedia* 2014;45:663–70. <https://doi.org/10.1016/j.egypro.2014.01.071>.
- [29] Bonalumi D, Giuffrida A. Investigations of an air-blown integrated gasification combined cycle fired with high-sulphur coal with post-combustion carbon capture by aqueous ammonia. *Energy* 2016;117:439–49. <https://doi.org/10.1016/j.energy.2016.04.025>.
- [30] Giuffrida A, Muioli S, Romano MC, Lozza G. Lignite-fired air-blown IGCC systems with pre-combustion CO<sub>2</sub> capture. *Int J Energy Res* 2016;40(6):831–45. <https://doi.org/10.1002/er.3488>.
- [31] Hou S, Wu Y, Zhou Y, Yu L. Performance analysis of the combined supercritical CO<sub>2</sub> recompression and regenerative cycle used in waste heat recovery of marine gas turbine. *Energy Convers Manage* 2017;151:73–85. <https://doi.org/10.1016/j.enconman.2017.08.082>.
- [32] Song J, Li XS, Ren XD, Gu CW. Performance improvement of a preheating supercritical CO<sub>2</sub> (S-CO<sub>2</sub>) cycle based system for engine waste heat recovery.

- Energy Convers Manage 2018;161:225–33. <https://doi.org/10.1016/j.enconman.2018.02.009>.
- [33] Thanganadar D, Asfand F, Patchigolla K. Thermal performance and economic analysis of supercritical carbon dioxide cycles in combined cycle power plant. *Appl Energy* 2019;255:113836. <https://doi.org/10.1016/j.apenergy.2019.113836>.
- [34] Liu Y, Zhao Y, Yang Q, Liu G, Li L. Thermodynamic comparison of CO<sub>2</sub> power cycles and their compression processes. *Case Studies in Thermal Engineering* 2020; 21:100712. <https://doi.org/10.1016/j.csite.2020.100712>.
- [35] Pan M, Zhu Y, Bian X, Liang Y, Lu F, Ban Z. Theoretical analysis and comparison on supercritical CO<sub>2</sub> based combined cycles for waste heat recovery of engine. *Energy Conversion and Management* 2020, 219:113049. [10.1016/j.enconman.2020.113049](https://doi.org/10.1016/j.enconman.2020.113049).
- [36] Pan P, Yuan C, Sun Y, Yan X, Lu M, Bucknall R. Thermo-economic analysis and multi-objective optimization of S-CO<sub>2</sub> Brayton cycle waste heat recovery system for an ocean-going 9000 TEU container ship. *Energy Convers Manage* 2020;221: 113077. <https://doi.org/10.1016/j.enconman.2020.113077>.
- [37] Li B, Wang SS, Wang K, Song L. Comparative investigation on the supercritical carbon dioxide power cycle for waste heat recovery of gas turbine. *Energy Convers Manage* 2021;228:113670. <https://doi.org/10.1016/j.enconman.2020.113670>.
- [38] Carraro G, Danieli P, Lazzaretto A, Boatto T. A common thread in the evolution of the configurations of supercritical CO<sub>2</sub> power systems for waste heat recovery. *Energy Convers Manage* 2021;237:114031. <https://doi.org/10.1016/j.enconman.2021.114031>.
- [39] Monje B, Sánchez D, Savill M, Pilidis P, Sánchez T. A Design Strategy for Supercritical CO<sub>2</sub> Compressors. *Proceedings of the ASME Turbo Expo* 2014. <https://doi.org/10.1115/GT2014-25151>.
- [40] Monge B, Sánchez D, Savill M, Sánchez T. Exploring the design space of the sCO<sub>2</sub> power cycle compressor, The 4th International sCO<sub>2</sub> Power Cycles Symposium, 2014, <http://sco2symposium.com/papers2014/turbomachinery/46-Sanchez.pdf>.
- [41] Allison TC, McClung A. Limiting Inlet Conditions for Phase Change Avoidance in Supercritical CO<sub>2</sub> Compressors. *Proceedings of the ASME Turbo Expo* 2019. <https://doi.org/10.1115/GT2019-90409>.
- [42] Persico G, Gaetani P, Romei A, Toni L, Bellobuono EF, Valente R. Implications of phase change on the aerodynamics of centrifugal compressors for supercritical carbon dioxide applications. *J Eng Gas Turbines Power* 2021;143(4):041007. <https://doi.org/10.1115/1.4049924>.
- [43] Allison TC, Moore J, Pelton R, Wilkes J, Ertas B. Turbomachinery, in “Brun K, Friedman P, Dennis R. (Eds.), Fundamentals and Applications of Supercritical Carbon Dioxide (SCO<sub>2</sub>) Based Power Cycles, Woodhead Publishing, 2017”, pp. 147–215, 10.1016/B978-0-08-100804-1.00007-4.
- [44] Wright S, Scammell W. Economics, in “Brun K, Friedman P, Dennis R. (Eds.), Fundamentals and Applications of Supercritical Carbon Dioxide (SCO<sub>2</sub>) Based Power Cycles, Woodhead Publishing, 2017”, pp. 127–145, 10.1016/B978-0-08-100804-1.00006-2.
- [45] Dixon SL, Hall CA. *Fluid Mechanics and Thermodynamics of Turbomachinery*. 7th edition. Butterworth-Heinemann; 2014.
- [46] Romei A, Gaetani P, Persico G. Design and off-design analysis of a highly loaded centrifugal compressor for sCO<sub>2</sub> applications operating in near-critical conditions. The 4th European sCO<sub>2</sub> Conference for Energy Systems 2021. <https://doi.org/10.17185/duerpublico/73969>.
- [47] Romei A, Gaetani P, Persico G. On sCO<sub>2</sub> compressor performance maps at variable intake thermodynamic conditions. *Proceedings of the ASME Turbo Expo* 2021. <https://doi.org/10.1115/GT2021-60252>.
- [48] Modekurti S, Eslick J, Omell B, Bhattacharyya D, Miller DC, Zitney SE. Design, dynamic modeling, and control of a multistage CO<sub>2</sub> compression system. *Int J Greenhouse Gas Control* 2017;62:31–45. <https://doi.org/10.1016/j.ijggc.2017.03.009>.
- [49] Lv G, Yang J, Shao W, Wang X. Aerodynamic design optimization of radial-inflow turbine in supercritical CO<sub>2</sub> cycles using a one-dimensional model. *Energy Convers Manag* 2018;165(March):827–39. <https://doi.org/10.1016/j.enconman.2018.03.005>.
- [50] Qi J, Reddell T, Qin K, Hooman K, Jahn IHJ. Supercritical CO<sub>2</sub> radial turbine design performance as a function of turbine size parameters. *J Turbomach* 2017; 139(8):081008. <https://doi.org/10.1115/1.4035920>.
- [51] Unglaube T, Chiang HWD. Preliminary Design of Small-Scale Supercritical CO<sub>2</sub> Radial Inflow Turbines. *J Eng Gas Turbines Power* 2020;142(2):021011. <https://doi.org/10.1115/1.4045273>.
- [52] Musgrove G, Sullivan S, Shiferaw D, Fourspring P, Chordia L. Heat exchangers in “Brun K, Friedman P, Dennis R. (Eds.), Fundamentals and Applications of Supercritical Carbon Dioxide (SCO<sub>2</sub>) Based Power Cycles, Woodhead Publishing, 2017”, pp. 217–244, 10.1016/B978-0-08-100804-1.00008-6.
- [53] Crespi F. *Thermo-Economic Assessment of Supercritical CO<sub>2</sub> Power Cycles for Concentrated Solar Power Plants*. University of Seville; 2019. Ph.D. Thesis.
- [54] Shiferaw D, Carrero JM, Le Pierres R. Economic analysis of sCO<sub>2</sub> cycles with PCHE recuperator design optimisation, The 5th International sCO<sub>2</sub> Power Cycles Symposium, 2016, <http://sco2symposium.com/papers2016/HeatExchanger/053paper.pdf>.
- [55] Kalra C, Hofer D, Sevincer E, Moore J, Brun K. Development of high efficiency hot gas turbo-expander for optimized CSP supercritical CO<sub>2</sub> power block operation, The 4th International sCO<sub>2</sub> Power Cycles Symposium, 2014, <http://sco2symposium.com/papers2014/turbomachinery/74-Kalra.pdf>.
- [56] Baldasso E, Mondejar ME, Larsen U, Haglind F. Regression models for the evaluation of the techno-economic potential of organic rankine cycle-based waste heat recovery systems on board ships using low sulfur fuels. *Energies* 2020;13(6): 1378. <https://doi.org/10.3390/en13061378>.
- [57] Lemmens S. Cost engineering techniques and their applicability for cost estimation of organic rankine cycle systems. *Energies* 2016;9(7):485. <https://doi.org/10.3390/en9070485>.
- [58] Noaman M, Awad O, Morosuk T, Tsatsaronis G, Salomo S. Identifying the Market Scenarios for Supercritical CO<sub>2</sub> Power Cycles. *J Energy Res Technol* 2022;144(5): 050906. <https://doi.org/10.1115/1.4052543>.